Supporting Information

Mariotti and Fagherazzi 10.1073/pnas.1219600110

SI Text

Physical Characteristics of Study Sites. Mean tidal ranges read 1.48 m for Cape May [Cape May, NJ–National Oceanic and Atmospheric Administration (NOAA) station 8536110], 1.22 m for the Virginia Coast Reserve (Wachapreague, VA–NOAA station 8631044), and 1.59 m for Charleston Sound (Charleston, SC–NOAA station 8665530). Relative sea-level rise (RSLR) along the Atlantic coast of the US during the late Holocene until the 20th century has been on the order of ∼2 mm/y, with slightly higher values along the New Jersey and Virginia coasts than in the Carolinas (1, 2). Wind regime is calculated considering three similar NOAA stations for the period 2005–2011: station CMAN4-8536110 for Cape May, station KPTV2-8632200 for Virginia Coast Reserve, and station FBIS1 for Charleston Sound. The 90th percentile of the hourly wind speed reads 7.6 m/s for Cape May, 8.2 m/s for Virginia Coast Reserve, and 8.8 m/s for Charleston Sound.

Analysis of Aerial Photographs. Two sets of rectified and georeferenced aerial photographs acquired between 1957 and 1959 (3) and between 2011 and 2012 (4) were used to assess the horizontal extension of the marsh basins, which were defined as rounded tidal flats surrounded by salt marshes for at least 270°. Using the Geographic Information System software QuantumGIS (5), the basins were manually identified using polygons with a side length of 1–100 m, depending on the regularity of the marsh boundary. The average horizontal migration rate of the marsh boundary was computed as the difference of the polygons' equivalent radius, equal to $\sqrt{A_f/\pi}$, divided by the time lapse of the two images. In addition, the characteristic depth of 10 marsh basins (see the numbered basins in Fig. 1 and Table S1) was extracted from available US Coast and Geodetic Survey charts.

Marsh Boundary Progradation. Marsh progradation results from vertical sedimentation over a gently sloping profile facing the marsh boundary (6). As a result, separating marsh progradation from tidal flat vertical accretion is an artificial step needed for simple point models like the one presented herein.

Marsh boundary progradation is modeled here as a mass-conserving redistribution of tidal flat sediments (see the first term in Eq. **2**). Sediments are subtracted from the tidal flat bottom and reallocated at the marsh boundary, where a gentle profile dissipates the incoming wave and the encroaching salt marsh vegetation enhances sediment trapping. This flux of sediment is computed assuming that the marsh boundary is a portion of tidal flat where all erosive process vanishes, and hence only deposition occurs:

$$B_a = w_s C_r \rho^{-1} \frac{1}{\tan(\varphi)}, \quad \textbf{[S1]}$$

where w_s is the settling velocity of the suspended sediments, C_r is the reference sediment concentration on the tidal flat, ρ is the dry sediment bulk density, and φ is the slope of the prograding marsh.

The marsh slope is a geometric feature emerging from the internal dynamics of the system and stems from the balance between sedimentation and erosion. Because we are not able to explicitly reproduce all physical processes that determine the geometry of the prograding marsh, the marsh slope becomes an external parameter in our model. For simplicity we rename $1/\tan(\varphi)$ as k_a, implying that k_a is a shape factor that represents the geometry of the marsh boundary. The value of k_a includes all of the other processes not explicitly taken into account in Eq. **S1**, such as the enhanced sediment trapping by vegetation. Here we use a reference value of $k_a = 2$, equivalent to a slope of 26°. A sensitivity analysis of the results with respect to k_a (equal to 1 for a slope of 45° and equal to 4 for a slope of 14°) is carried out when the parameter optimization is performed (Fig. S4).

Because k_a is dictated by the mechanism of sediment trapping, it is unlikely that it varies among the three sites, which are characterized by similar salt marshes (dominated by *Spartina spp*, ref. 7). A full numerical model for the coupled evolution of salt marshes and tidal flats indicates that the marsh progradation rate increases linearly with sediment concentration, hence supporting our simplified formulation (6). Unfortunately, because the results of the full model include the effect of wave-induced marsh erosion, extracting a parametrization for marsh progradation alone is not possible.

The simplified model predicts a marsh boundary progradation rate, in the absence of marsh erosion, equal to 0.5 m·y^{-1} for a concentration of 30 mg/L and to 2 m·y^{-1} for a concentration of 120 mg/L, using the reference values for k_a (equal to 2), w_s (0.5 mm/s, ref. 8) and ρ (1,000 kg/m^3). In the full model, where a fixed fetch and wind regime are considered, marsh progradation rates of 0.5 and 2 m·y^{-1} are achieved for concentrations of ∼400 and ∼900 mg/L, respectively.

Waves on Tidal Flats. To compute the significant wave height H_s and the peak wave period T_p on the tidal flats, we use semi-empirical equations (9):

$$\frac{gH_s}{(U_{wind})^2} = 0.2413\left\{\tanh A_1 \tanh\left[\frac{B_1}{\tanh A_1}\right]\right\}^{0.87}$$
$$\frac{gT_p}{U_{wind}} = 7.518\left\{\tanh A_2 \tanh\left[\frac{B_2}{\tanh A_2}\right]\right\}^{0.37}, \quad \textbf{[S2]}$$

with $A_1 = 0.493(gd/[U_{wind}]^2)^{0.75}$, $B_1 = 3.13 \times 10^{-3}(g\chi/[U_{wind}]^2)^{0.57}$, $A_2 = 0.331\ (gd/[U_{wind}]^2)^{1.01}$, $B_2 = 5.215 \times 10^{-4}(g\chi/[U_{wind}]^2)^{0.73}$, where d is the depth, χ is the fetch, and U_{wind} is the reference wind speed.

We consider a fetch equal to the basin width and a depth equal to the average between the minimum and maximum water depth on the tidal flat, $d = [h + \max(0, h - r)]/2$. The wave bed shear stress τ_w is computed, using the linear wave theory, as $\tau_w = 1/2\rho f_w(\pi H_s/[T_p \sinh(kh)])^2$, where k is the wave number, calculated via the dispersion relationship, f_w is a friction factor, set equal to $f_w = 0.4[H_s/\sinh(kh)/k_o]^{-0.75}$, where the roughness k_o is set equal to 1 mm.

The reference concentration in the basin is set equal to $C_r = \rho\lambda S/(1+\lambda S)$ (10), where λ is a nondimensional coefficient representing the sediment erodability, set equal to 10^{-4}, $S = (\tau_w - \tau_{cr})/\tau_{cr}$ is the excess shear stress, and τ_{cr} is the critical shear stress, equal to 0.1 Pa (8).

Waves at the Marsh Boundary. Generalizing an empirical tidal flat profile (11), we assume that the bed level in front of the marsh is equal to $h_x(x) = h_m + (h - h_m)(1 - \exp[0.1\ x/h])$, where x is the distance from the marsh boundary. We then assume that the shoaling bottom profile in front of the marsh ends at a fixed distance $x = x_{ref}$, set equal to 10 m, obtaining $h_b = h_m + (h - h_m)(1 - \exp[1/h])$.

Because of the sloping bed in front of the marsh boundary, waves reaching the marsh scarp differ from those on the open tidal flat. The wave power density at the marsh boundary is hence computed as

$$W=\frac{\gamma}{16}c_g[H_{sb}]^2, \qquad \textbf{[S3]}$$

where H_{sb} and $c_g=\frac{2\pi}{k_b T_{pb}}\frac{1}{2}\left(1+\frac{2k_b h_b}{\sinh(2k_b h_b)}\right)$ are the wave height and the group velocity at the base of the marsh scarp, and k_b and T_{pb} are the wave number and wave period, respectively.

The wave energy at the marsh scarp should be computed by propagating tidal flat waves along the shoaling profile facing the marsh boundary. Given the uncertainty on the bed profile, we do not explicitly compute wave propagation. Instead, we estimate the wave energy at the marsh scarp by using the same semiempirical equations adopted to compute the wave energy on the tidal flat (9) substituting h with h_b. A similar approach, in which wave characteristics in front of the marsh boundary are computed by using Eq. **S2**, has already been adopted (12).

The resulting wave power is sensitive to the choice of bed profile and reference distance used to compute h_b. The greater the reference distance to compute the wave power at the marsh scarp, the greater the resulting wave power. This is a model limitation, which we believe is common to all models that predict wave regime. For example, high-resolution models that compute wave power at the marsh boundary necessarily approximate the slope in front of the marsh with few cells, and hence the choice of the reference cell representing the marsh boundary will influence the computed wave power.

Rates of Erosion. Even though the width of the marsh basin tends to infinite, a finite depth is reached when the fetch-unlimited condition is attained. Fig. S1 shows that the basin reaches the fetch-unlimited condition for a width of ∼100 km, but the asymptotic migration rate is attained for fetch of ∼10 km because of the wave attenuation at the marsh boundary.

The fetch-unlimited equilibrium tidal flat depth is reached for large widths (>100 km), values greater than those predicted by previous point models (13–15). This difference springs from taking into account the effect of fetch on wave period and hence on bed shear stresses (16), a dependence neglected in precedent models (13–15).

Case with Fixed Fetch. Basin expansion stops when all of the marsh is eroded and the fetch is determined by the size and shape of the bay. In this scenario the system reduces to

$$\frac{dh}{dt}=\frac{\min[r,h](C_r-C_o)}{T_{\omega}\rho}+R. \qquad \textbf{[S4]}$$

For a fixed set of parameters (R, C_o, and w), the system admits a single stable equilibrium. The equilibrium depth is reported in Fig. S2 as a function of w and C_o.

In our model the tidal flat depth quickly adapts to the width, as shown by the fact that the unstable manifold quickly attracts all trajectories, leading to an almost univocal correspondence between width and depth. As a result, one-point models (13–15) remain valuable tools for the predictions of the tidal flat depth.

Optimal Values for the Parameters C_o and k_e. The root-mean-square error (RMSE) of the migration rate for each site is computed as

$$\mathrm{RMSE}=\sqrt{\sum\frac{(O-M)^2}{n}}, \qquad \textbf{[S5]}$$

where O are the observed rates, M are the measured rates, and n is the number of basins at each site.

The RMSE is computed by varying the parameters C_o and k_e and by keeping all of the other parameters fixed. The optimization is first performed assuming k_a is equal to 2 (Fig. S3), and then assuming k_a is equal to 1 and 4 (Fig. S4). Optimal values of C_o and k_e, associated with the minimum RMSE, are reported in Table S3.

1. Engelhart SE, Horton BP, Douglas BC, Peltier WR, Törnqvist TE (2009) Spatial variability of late Holocene and 20th century sea-level rise along the Atlantic coast of the United States. *Geology* 37(12):1115–1118.
2. Sallenger AH, Doran KS, Howd PA (2012) Hotspot of accelerated sea-level rise on the Atlantic coast of North America. *Nat Clim Change* 2:884–888.
3. US Geological Survey (2012) Aerial Photography Single Frame Records. Available at http://eros.usgs.gov/#/Find_Data/Products_and_Data_Available/Single_Frame_Records.
4. US Department of Agriculture, Farm Service Agency (2012) National Agriculture Imagery Program. Available at www.fsa.usda.gov/FSA/apfoapp?area=home&subject=prog&topic=nai.
5. Quantum GIS Development Team (2012) Quantum GIS Geographic Information System. Open Source Geospatial Foundation Project. Available at http://qgis.osgeo.org.
6. Mariotti G, Fagherazzi S (2010) A numerical model for the coupled long-term evolution of salt marshes and tidal flats. *J Geophys Res* 115:F01004.
7. Bertness MD (1998) *The Ecology of Atlantic Shorelines* (Sinauer, Sunderland, MA), 417 pp.
8. Lawson SE, Wiberg PL, McGlathery KJ, Fugate DC (2007) Wind-driven sediment suspension controls light availability in a shallow coastal lagoon. *Estuaries Coasts* 30(1):102–112.
9. Young IR, Verhagen LA (1996) The growth of fetch limited waves in water of finite depth. 1. Total energy and peak frequency. *Coast Eng* 29:47–78.
10. Smith JD, McLean DR (1977) Spatially averaged flow over a wavy surface. *J Geophys Res* 82:1735–1746.
11. Wilson CA, Allison MA (2008) An equilibrium profile model for retreating marsh shorelines in southeast Louisiana. *Estuar Coast Shelf Sci* 80(4):483–494.
12. Tambroni N, Seminara G (2012) A one-dimensional eco-geomorphic model of marsh response to sea level rise: Wind effects, dynamics of the marsh border and equilibrium. *J Geophys Res* 117:F03026.
13. Fagherazzi S, Carniello L, D'Alpaos L, Defina A (2006) Critical bifurcation of shallow microtidal landforms in tidal flats and salt marshes. *Proc Natl Acad Sci USA* 103(22): 8337–8341.
14. Marani M, D'Alpaos A, Lanzoni S, Carniello L, Rinaldo A (2007) Biologically-controlled multiple equilibria of tidal landforms and the fate of the Venice lagoon. *Geophys Res Lett* 34:L11402.
15. Marani M, D'Alpaos A, Lanzoni S, Carniello L, Rinaldo A (2010) The importance of being coupled: Stable states and catastrophic shifts in tidal biomorphodynamics. *J Geophys Res* 115:F04004.
16. Mariotti G, Fagherazzi S (2013) Wind waves on a mudflat: The influence of fetch and depth on bed shear stress. *Cont Shelf Res*, Special Issue: Tidal flats, 10.1016/j.csr.2012.03.001.

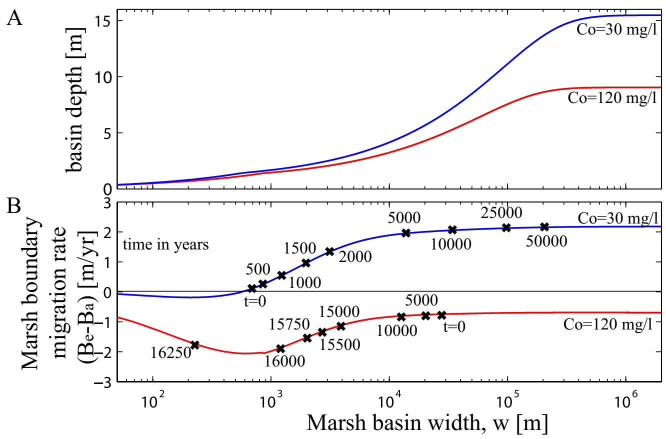

Fig. S1. (*A*) Basin depth as a function of marsh basin width, following the trajectory on the unstable manifold, for two different values of concentration (30 and 120 mg/L), with r = 1.4 m, k_a= 2, k_e= 0.1 m^3·y^{-1}·W^{-1}, RSLR = 2 mm/y, U_{wind} = 8 m/s. (*B*) Marsh boundary migration rate (positive if retreating) as a function of marsh basin width. For C_o = 30 mg/L there is a critical basin width and the migration rate tends toward an asymptotic positive value for large widths. For C_o = 120 mg/L the critical basin width is not present and the basin is always contracting (negative migration rate). Crosses represent points along the two trajectories at various times.

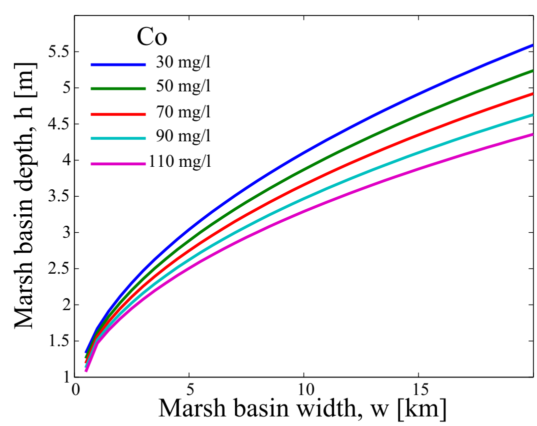

Fig. S2. Equilibrium depth as function of a fixed basin width (Eq. **S4**), for different values of C_o. Parameter values: r = 1.4 m, k_a = 2, k_e = 0.1 m^3·y^{-1}·W^{-1}, RSLR = 2 mm/y, U_{wind} = 8 m/s.

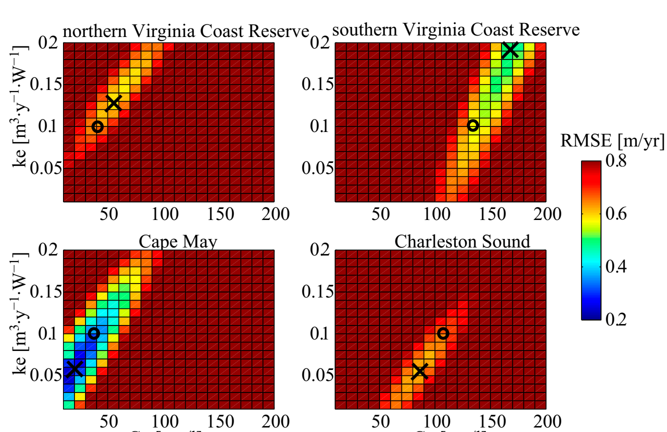

Fig. S3. RMSE of the boundary migration rate as a function of C_o and k_e, for the four sites, with k_a = 2 (reference value). Crosses indicate the optimal combination (i.e., associated with the smallest RMSE) of C_o and k_e. Circles indicate the optimal value of C_o fixing k_e to 0.1 m^3·y^{-1}·W^{-1}. Parameter values: r = 1.4 m, RSLR = 2 mm/y, U_{wind} = 8 m/s.

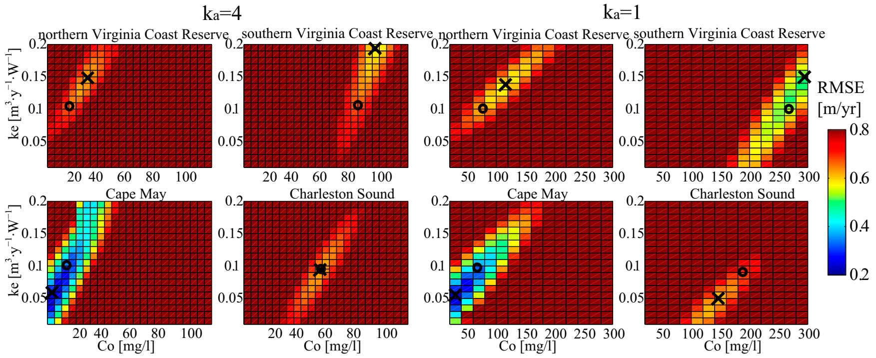

Fig. S4. RMSE of the boundary migration rate as a function of C_o and k_e for the four sites, with two different values of k_a: 4 and 1. Parameter values: $r = 1.4$ m, RSLR = 2 mm/y, U_{wind} = 8 m/s.

Table S1. Available basin widths and depths (same as Fig. 2)

Basin no.	Depth, m	Width, m	Basin name	Ref(s).
1	1.52	1,453	Jarvis Sound (Cape May, NJ)	(1)
2	1.77	1,622	Richardson Sound (Cape May, NJ)	
3	1.78	1,972	Jenkins Sound (Cape May, NJ)	
4	2.07	2,908	Great Sound (Cape May, NJ),	
5	1.52	1,299	Stites Sound (Cape May, NJ),	
6	1.83	1,418	Townsend Sound (Cape May, NJ)	
7	1.68	1,871	Gray Bay (Charleston Sound, SC)	(2)
8	1.83	2,551	Copahee Sound (Charleston Sound, SC)	
9	1.83	1,251	Mark Bay (Charleston Sound, SC)	
10	2.01	2,296	Swee Bay (Charleston Sound, SC)	

1. Lucke JB (1934) Tidal inlets: A theory of evolution of lagoon deposits on shorelines of emergence. *J Geol* 42:561–584.
2. US Coast and Geodetic Survey (1909) Coast Chart No. 153. North Island to Isle of Palms including Cape Romain (SC).

Table S2. Basin width and marsh boundary migration rate (as in Fig. 4)

Width, m	Marsh boundary migration, m/y	Location
521	−0.80514	Northern Virginia Coast Reserve (VA)
1,155	1.086036	
3,396	1.684828	
390	−1.63868	
286	−0.52315	
262	−1.32535	
2,281	0.977636	
4,232	1.062644	
951	0.069372	
2,816	1.604314	
560	0.539177	
1,510	0.295826	
1,424	0.092268	
1,198	0.569737	
10,547	1.763794	
845	−0.85557	
190	−0.12603	
1,383	1.34918	
1,165	−1.80779	Southern Virginia Coast Reserve (VA)
978	−2.3569	
626	−2.29373	
469	−2.19819	
442	−2.54257	
207	−1.85919	

Table S2. Cont.

Width, m	Marsh boundary migration, m/y	Location
404	−3.73292	
726	−2.19157	
1,453	1.066672	Cape May (NJ)
623	0.402494	
1,622	0.410876	
99	−0.24449	
1,847	0.361717	
619	0.234307	
1,972	0.357643	
2,908	0.553143	
524	0.073716	
1,299	0.438171	
393	−0.12149	
1,418	0.565365	
2,272	0.708857	
829	0.259268	
432	−0.35542	
213	0.24543	
1,871	−0.84743	Charleston Sound (SC)
2,551	−1.43541	
1,251	−1.04167	
664	−1.88384	
2,296	−2.80707	
192	−1.54767	
756	−1.13803	
882	−0.91713	
283	−0.86803	
141	−0.82888	
193	−1.38745	
9,507	−0.23384	

Table S3. Optimal value of k_e and C_o for different values of k_a

	$k_a = 2$			$k_a = 1$			$k_a = 4$		
Site name	k_e	C_o	C_o*	k_e	C_o	C_o*	k_e	C_o	C_o*
North VCR	0.14	60	30	0.14	120	70	0.14	25	20
Cape May	0.06	20	30	0.05	20	60	0.06	10	20
South VCR	0.19	170	130	0.15	300	270	0.19	90	80
Charleston	0.06	80	110	0.06	150	180	0.1	60	60

C_o* is the optimal value of C_o assuming k_e is equal to 0.1. The unit of C_o is mg/L, the unit of k_e is $m^3 \cdot y^{-1} \cdot W^{-1}$. VCR, Virginia Coast Reserve.